AGU ADVANCING EARTH AND SPACE SCIENCES

Geophysical Research Letters®

RESEARCH LETTER
10.1029/2023GL107381

Key Points:

- An advanced shear-current modified nonlinear Schrödinger-type equation is derived for surface waves in a background open-ocean flow
- The interplay between Stokes drift, background flow, and Eulerian return flow by a wave group, in extreme waves generation is revealed
- How a background flow suppresses the modulational instability is explained and its relevance to the CL2 instability is discussed

Supporting Information:

Supporting Information may be found in the online version of this article.

Correspondence to:

Y. Li,
yan.li@uib.no

Citation:

Li, Y., & Chabchoub, A. (2024). How currents trigger extreme sea waves. The roles of Stokes drift, Eulerian return flow, and a background flow in the open ocean. *Geophysical Research Letters*, *51*, e2023GL107381. https://doi.org/10.1029/2023GL107381

Received 17 NOV 2023
Accepted 9 FEB 2024

Author Contributions:

Conceptualization: Yan Li
Formal analysis: Yan Li
Funding acquisition: Yan Li, Amin Chabchoub
Investigation: Yan Li
Methodology: Yan Li, Amin Chabchoub
Project administration: Yan Li
Resources: Yan Li
Validation: Yan Li, Amin Chabchoub
Visualization: Yan Li
Writing – original draft: Yan Li
Writing – review & editing: Yan Li, Amin Chabchoub

How Currents Trigger Extreme Sea Waves. The Roles of Stokes Drift, Eulerian Return Flow, and a Background Flow in the Open Ocean

Yan Li[1,2] **and Amin Chabchoub**[3,4]

[1]Department of Mathematics, University of Bergen, Bergen, Norway, [2]Bjerknes Centre for Climate Research, University of Bergen, Bergen, Norway, [3]Hakubi Center for Advanced Research, Disaster Prevention Research Institute, Kyoto University, Kyoto, Japan, [4]School of Civil Engineering, The University of Sydney, Sydney, NSW, Australia

Abstract A deterministic system of ocean surface waves and flow in the oceanic boundary layer is key to understanding the dynamics of the upper ocean. For the description of such complex systems, a higher-order shear-current modified nonlinear Schrödinger equation is newly derived and then used to physically interpret the interplay between Stokes drift, Eulerian return flow due to a passing wave group, and an open-ocean vertically sheared flow in the extreme sea wave generation. The conditions for the suppression or enhancement of the modulation instability in the rogue wave dynamics in the presence of a background flow are reported, whose relevance and influence to the Craik-Leibovich type 2 instability in triggering a Langmuir-type circulation is discussed. The findings highlight the need for future studies to establish and assess the energy transfer from waves to currents or in the reversing order, asserting a plausible physical mechanism for the dissipation of the surface wave energy through wave-current interactions in the open ocean.

Plain Language Summary The dynamics of the upper-ocean involve many complex processes, including for instance the interplay between wind, waves, currents, and global circulation systems. Such interactions can give rise to instabilities and extreme events with far-reaching consequences. In this letter, we use a newly derived weakly nonlinear wave framework accounting for the presence of shear currents to quantify the requirements to trigger modulation instability, giving rise to long-crested rogue waves. Our investigation also provides combined conditions for the occurrence of both, modulation and Craik-Leibovich (type 2) instabilities, and demonstrates the possibility of energy transfers between waves as well as between waves and currents in the ocean.

1. Introduction

Surface waves are ubiquitous in the open ocean. They interact with both small- and large-scale open-ocean flows, for example, tidal, wind-induced, and submesoscale currents, which has led to both, influencing ocean circulations (McWilliams, 2016; Suzuki & Fox-Kemper, 2016) and altered properties as a result of interactions with currents. The latter is the focus of this study in which we devote a particular focus on the relevance of such interplay on global circulation processes.

The approximate scale ranges for the wavelength of surface gravity waves are typically within 0.10–100 m which means wave-induced oscillating motions are much more rapid and shorter in length than those induced by upper ocean flows (Suzuki & Fox-Kemper, 2016; Toffoli & Bitner-Gregersen, 2017; L. Wu et al., 2019). The much smaller scales of surface waves, compared to other processes in the ocean, demand extra computing powers to represent their effects in larger scale regional and global models for oceanic flows. For a better efficiency, surface waves have been represented in the last three decades in a wave-phase averaged manner in newly developed asymptotic theories and models for ocean circulations (McWilliams et al., 2004; Mellor, 2016; Suzuki & Fox-Kemper, 2016), also known as wave-averaged effects in the wave-current interaction framework. This in particular permits the consideration of long-term and slowly varying features of surface waves to be physically resolved, albeit short and rapidly varying scales compared with upper ocean flows (D'Asaro, 2014).

The phase-averaged effects of infinitesimal waves are represented in the form of Stokes drift in a few ocean models (Ardhuin et al., 2008; Breivik et al., 2014; Lane et al., 2007; Madec et al., 2017; McWilliams et al., 2004; Shchepetkin & McWilliams, 2005), which lead to the coupling with a current in a leading-order approximation as

a combination of vortex force and adjusted pressure (Suzuki & Fox-Kemper, 2016), while there are other ocean models which physically interpret these effects in the form of radiation stress (Babanin & Chalikov, 2012; Longuet-Higgins & Stewart, 1962; Mellor, 2015, 2016; Qiao et al., 2010). Following Craik and Leibovich (1976), the Stokes drift is considered contributing to an instability mechanism for the generation of Langmuir circulation, also known as the Craik-Leibovich type 2 (CL2) mechanism. It is widely investigated to model and understand the dynamics of upper ocean flows (Leibovich, 1983; McWilliams et al., 2004; van den Bremer & Breivik, 2018). Stokes drift profiles are primarily parameterized in ocean models, see, for example, Breivik et al. (2014, 2016), Breivik and Christensen (2020), and S. F. Zippel et al. (2022) among others. Therefore, it is evident that surface waves play a role as an external driving source in such ocean models. This role implies that the respective ocean flows should consist of a part that is highly correlated to the Stokes drift, such as in the case of waves in a stratified fluid (Higgins et al., 2020) or depth dependent flow (Zheng et al., 2024), which is referred to as the *wave-modified background flow* and detectable through in situ findings by Smith (2006). Note that the drift processes near the ocean surface are largely driven by short waves, which are not accurately modeled in the operational wave forecast models (Janssen & Bidlot, 2018). A key observation by Smith (2006) is the higher correlation between Eulerian flows and Stokes drift, being much stronger than those forced by second-order surface waves alone. Indeed, a wave-modified background flow differs physically from the wave-induced Eulerian return flow as generated from a passing wave group. The former requires the additional presence of a background flow, whereas the latter does not and has been extensively studied in the framework of potential flow theory, see for example, Dysthe (1979), McIntyre (1981), Pizzo and Melville (2016), van den Bremer et al. (2019), and Li & Li (2021). A wave-modified background flow defined here in an Eulerian frame differs from a Lagrangian mean flow in studies using a Lagrangian frame. In this latter work, the authors have rigorously quantified the unidirectional physical wave behavior resulting from a kinematic constraint on the fluid's vorticity. How such a wave-modified background flow affects the evolution of surface waves, and to the best of our knowledge, has not been physically elucidated and will be rigorously addressed in this work. Through our study, we especially demonstrate that a wave-modified background flow plays a key role in both, suppressing or enhancing the formation of abnormally large waves caused by an instability mechanism called Modulational Instability (MI), which has been widely known in both, optics and hydrodynamics (Dudley et al., 2019; Fujimoto et al., 2019). Here, we derive a combined criterion in which the exponential growth of wave amplitude and the CL2 instability can be both met. This may provide novel physical insights into the possible relationship between growing waves and intense Langmuir circulations as discussed in Phillips (2002).

Rogue waves, which belong to a type of extremely large sea wave events in natural hazard classifications, have been measured in the world's oceans and are thereby well-documented. They are referred to as those that appear unexpectedly and have a much larger amplitude or height than their surrounding waves (Kharif & Pelinovsky, 2003). Both, the MI and wave-current interaction have been recognized as a possible mechanism of their formation (Janssen, 2003; Kharif & Pelinovsky, 2003; Trulsen et al., 2000). The MI, in principle, attributes to the combined physics of (quasi-) quartet wave interaction and third-order nonlinearity in wave steepness, which can be described by the nonlinear Schrödinger equation (NLS) in the case of narrow energy spectrum (Benjamin, 1967; Chabchoub et al., 2011; Onorato et al., 2009; Zakharov, 1968). Rogue wave events have been observed to be triggered at seas in the presence of strong currents, for example, the Gulf Stream and Agulhas Current (Lavrenov, 1998; Peregrine, 1976; White & Fornberg, 1998). A current being assessed as “weak” or “strong” depends on its wavenumber-weighted velocity magnitude compared with the phase velocity of waves (Banihashemi & Kirby, 2019; Ellingsen & Li, 2017; Quinn et al., 2017; Shrira, 1993). Strong currents can lead to the refraction and spatial focusing of waves (White & Fornberg, 1998). When nonlinear effects are at play, the spatial gradients of the profile of spatially varying currents can particularly lead to the energy transfer from current to waves using a current-amended NLS for water waves as the model (Hjelmervik & Trulsen, 2009; Onorato et al., 2013). In fact, it has been reported that the significant wave height is considerably amplified in the presence of strong opposing currents in experiments (Toffoli et al., 2015; Zhang et al., 2023), theoretical and numerical simulations (Zheng et al., 2023), and in situ observations (Romero et al., 2017; S. Zippel & Thomson, 2017). The three-dimensional Doppler shift of a weak current on the linear dispersion relation of waves has been well-studied and incorporated into wave models (Banihashemi & Kirby, 2019; Cavaleri et al., 2018). In all the aforementioned studies, the current in the form of a wave-altered background flow has not been so far considered in triggering rogue wave events, even in two-way coupling models. This is likely due to the fact that wave phases cannot be resolved in coupled wave and circulation models. As noted earlier, we aim to fill in this knowledge gap as is going to be elaborated upon in the next sections.

2. Methods

2.1. Problem Statement and Perturbation Expansion

We start with the problem statement for a system consisting of three-dimensional surface gravity waves and an open-ocean flow. The origin of the vertical axis z is placed on a still water surface given by $z = 0$, and the elevation of the free water surface is $z = \zeta(\mathbf{x}, t)$, where ζ denotes the surface elevation and $\mathbf{x} = (x, y)$ together with t denote the position vector in the horizontal plane and time, respectively. The main propagation direction of the waves is in the direction of the carrier wave vector $\mathbf{k}_0$ which is following the positive x axis, thereby, $\mathbf{k}_0 = (k_0, 0)$ and $\mathbf{k}_0 \times \mathbf{x} = 0$ for k_0 denoting the carrier wavenumber. The wave-induced velocity is described by $\mathbf{V}(\mathbf{x}, z, t) = [\mathbf{u}(\mathbf{x}, z, t), w(\mathbf{x}, z, t)]$, while $\mathbf{u}$ and w denote the wave-induced velocity vector in the horizontal plane and vertical velocity, respectively.

On the other hand, the characteristic properties of the background flow are in principle assumed relative to the scales of the carrier wave. The velocity of the background flow is described by $\boldsymbol{\mathcal{U}}(\boldsymbol{\chi}, z, \tau)$ where $\boldsymbol{\chi}$ and τ are slowly varying position vectors in the horizontal plane and time, respectively, such that $\boldsymbol{\chi} \sim \alpha\mathbf{x}$ and $\tau \sim \beta t$. The variables $\alpha \ll 1$ and $\beta \ll 1$ are dimensionless scaling parameters. Let $\boldsymbol{\mathcal{U}} = (\mathbf{U}_b, W)$ with $\mathbf{U}_b(\boldsymbol{\chi}, z, \tau)$ and $W(\boldsymbol{\chi}, z, \tau)$ being the velocity vector in the horizontal plane and the vertical velocity, respectively. Assuming an incompressible flow, negligible viscosity, and Coriolis force, the fluid system of surface waves in a large-scale flow is described by the continuity and Euler momentum equations given by

$$\nabla_3 \cdot (\mathbf{V} + \boldsymbol{\mathcal{U}}) = 0, \tag{1a}$$

$$\partial_t(\mathbf{V} + \boldsymbol{\mathcal{U}}) + [(\mathbf{V} + \boldsymbol{\mathcal{U}}) \cdot \nabla_3](\mathbf{V} + \boldsymbol{\mathcal{U}}) + \nabla_3(P - \rho g z)/\rho = 0. \tag{1b}$$

Here, $\nabla_3 = (\nabla, \partial_z)$ denotes the spatial gradient operator in three dimensions with $\nabla = (\partial_x, \partial_y)$ the gradient operator in the horizontal plane, ρ denotes the water density which is assumed constant, g denotes the gravitational acceleration, and $P(\mathbf{x}, z, t)$ is the pressure, which is expressed in a form of $P = P_w(\mathbf{x}, z, t) + P_b(\mathbf{x}, z, t)$, with P_w and P_b the pressure due to waves and the background flow, respectively. The system is described by the dynamic and kinematic boundary conditions at the free water surface $z = \zeta$, and the deep-water boundary condition, respectively,

$$P - \rho g z = 0 \text{ and } \partial_t \zeta + (\mathbf{u} + \mathbf{U}_b) \cdot \nabla\zeta = w + W; \tag{2a, b}$$

$$(\mathbf{V} + \boldsymbol{\mathcal{U}}) \to \mathbf{0} \text{ as } z \to -\infty. \tag{3}$$

The multiple-scales approximate solution to the boundary value problem described by Equations 1–3 are obtained with additional assumptions detailed in the following sections.

The potential flow theory has been widely recognized in accurately describing the motions induced by surface waves in the open ocean. Nevertheless, this becomes inapplicable in the additional presence of a background flow owing to that the flow can modify the wave motions to become rotational (see, e.g., Craik and Leibovich (1976); McWilliams et al. (2004)). To account for both, the rotational and irrotational components, the velocity of the wave-induced motions is expressed in a form as follows

$$\mathbf{V} = \nabla_3\phi(\mathbf{x}, z, t) + \mathbf{V}_r(\mathbf{x}, z, t), \tag{4}$$

where $\phi(\mathbf{x}, z, t)$ denotes the velocity potential and accounts for the irrotational flow motions, and $\mathbf{V}_r$ denotes the velocity of the wave-induced rotational motions which can lead to non-vanishing vorticity, that is, $\nabla_3 \times \mathbf{V}_r \neq \mathbf{0}$. Following a perturbation expansion, the unknown wave-perturbed fields in the description of the boundary value problem by Equations 1–3 are found in the form of power series in wave steepness ε as follows

$$\zeta = \sum_{j=1}^{3} \varepsilon^j \zeta^{(j)}, \ \phi = \sum_{j=1}^{3} \varepsilon^j \phi^{(j)}, \mathbf{V}_r = \mu_0 \sum_{j=1}^{3} \varepsilon^j \mathbf{V}_r^{(j)}, \tag{5}$$

being truncated up to the third-order. The superscripts "(j)" denotes $\mathcal{O}(\varepsilon^j)$, and μ_0 denotes the leading order of magnitude of the velocity of the background flow.

Using the characteristic velocity U_c, length L_c, and period T_c, we assume the leading-order scales of the profile dependence of the background flow in the horizontal plane and time below, regardless of its correlation to the waves. Following the dimensionless analysis and taking into account the continuity equation for the background flow, we obtain

$$|\nabla \mathbf{U}_b| \sim \alpha\mu_0 U_c/L_c, |\partial_t \mathbf{U}_b| \sim \beta\mu_0 U_c/T_c, \text{ and } W \sim \alpha^2\mu_0 U_c, \tag{6a, b, c}$$

where the scaling of Equation 6 used the widely utilized assumption for geophysical flows that the horizontal length of the flow is an order of magnitude higher than the vertical one and the temporal scale depends on a time much slower than the characteristic period T_c.

The linearized boundary value problem for wave-induced motions (see Text S1.1 in Supporting Information S1 for details) can be obtained based on Equations 1–3, which requires additional initial conditions to be properly solved. To this end, two types of initial conditions are typical; surface elevation prescribed in space at an initial instant, for example, data measured from sea surface stereo images or satellites (Guimarães et al., 2020), or a record of time series of the surface elevation measured at a fixed position, for example, measurements from single-point wave buoys (Ribal & Young, 2019). In both cases, the linear elevation admits a general expression as follows

$$\zeta^{(1)}(\mathbf{x},t) = \int \hat{\zeta}^{(1)}(\mathbf{k},0)\mathrm{e}^{\mathrm{i}\psi(\mathbf{x},t)}\mathrm{d}\mathbf{k}. \tag{7}$$

Here, $\psi(\mathbf{x}, t; \mathbf{k}, \omega) = \mathbf{k}\cdot\mathbf{x} - \omega t$ denotes the wave phase of the monochromatic wave with vector and angular frequency given by $\mathbf{k}$ and ω, respectively. Moreover, $\hat{\zeta}^{(1)}(\mathbf{k},0)$ denotes the Fourier transform of surface elevation at $t = 0$ s and $\hat{\zeta}^{(1)}(\mathbf{k},t) = \hat{\zeta}^{(1)}(\mathbf{k},0)\exp(-\mathrm{i}\omega t)$ denotes the Fourier transform of $\zeta^{(1)}$ at an arbitrary time instant. Inserting the surface elevation expression into the linearized kinematic boundary condition from Equation 2b leads to the vertical velocity in the form as (Li & Ellingsen, 2019)

$$w^{(1)}(\mathbf{x},z,t) = \int \mathrm{i}(\mathbf{k}\cdot\mathbf{U}_b(z=0) - \omega)\hat{\zeta}(\mathbf{k})\hat{w}^{(1)}(\mathbf{k},z)\mathrm{e}^{\mathrm{i}\psi}\mathrm{d}\mathbf{k}, \tag{8}$$

where the linear vertical velocity $w^{(1)}(\mathbf{x},z,t) = \partial_z\phi^{(1)} + w_r^{(1)}$, $\hat{w}(\mathbf{k},z)$ denotes the dimensionless vertical velocity which depends on depth z, and $\hat{w}(\mathbf{k},0) = 1$ by definition. Substituting the expression for the linear vertical velocity into the linearized boundary value problem based on (2.1)–(3) gives rise to

$$(\mathbf{k}\cdot\mathbf{U}_b - \omega)\left(\partial_{zz} - k^2\right)\hat{w}^{(1)}(\mathbf{k},z) - \mathbf{k}\cdot\mathbf{U}_b''\hat{w}^{(1)}(\mathbf{k},z) = 0 \text{ for } -\infty \le z \le 0 \tag{9a}$$

$$(\omega - \mathbf{k}\cdot\mathbf{U}_b)^2\partial_z\hat{w}^{(1)} - \left[gk^2 - (\omega - \mathbf{k}\cdot\mathbf{U}_b)\,\mathbf{k}\cdot\mathbf{U}_b'\right]\hat{w}^{(1)} = 0 \text{ for } z = 0, \tag{9b}$$

$$\hat{w} \to 0 \text{ for } z \to -\infty, \tag{9c}$$

see, for example, Li and Ellingsen (2019). Here, the prime denotes the derivative with respect to z (i.e., $\mathbf{U}' = \partial_z\mathbf{U}$ and $\mathbf{U}'' = \partial_{zz}\mathbf{U}$). Following Stewart and Joy (1974), Kirby and Chen (1989), Shrira (1993), and Ellingsen & Li (2017), the boundary value problem described by Equations 9a–9c leads to the *approximate current-modified dispersion relation* under the assumption of weak current, given by

$$\omega(\mathbf{k}) = \sqrt{gk}\left(1 + \sqrt{k/g}\,\tilde{U}_b\right) \text{ with } \tilde{U}_b(\mathbf{k},\chi,\tau) = \int_{-\infty}^{0} 2\mathbf{k}\cdot\mathbf{U}_b(\chi,\xi,\tau)\mathrm{e}^{2k\xi}\mathrm{d}\xi, \tag{10a, b}$$

where $\tilde{U}_b(\mathbf{k},\chi,\tau)$ is interpreted as the leading-order effect of the large-scale open flow, which is depth- and wavenumber-weighted. The dispersion relation given by Equation 10a is applicable when the latter depth- and

wavenumber-weighted velocity $\tilde{U}_b$ is small compared to the phase velocity $\sqrt{g/k}$, which leads to a non-dimensional velocity defined as

$$\mathcal{U}(\mathbf{k};\boldsymbol{\chi},\tau) \equiv \sqrt{k/g}\ \tilde{U}_b(\mathbf{k}) \text{ with } |\mathcal{U}| \ll 1. \tag{11}$$

The dimensionless velocity given by Equation 11 suggests that $\mathcal{O}(\mathcal{U}) \sim \mu_0 \ll 1$ is assumed hereafter, implying $U_c = \sqrt{g/k}$ was used. This assumption indicates the difference in the applicability regime of the derivations from Thomas et al. (2012). In this latter pioneering theoretical work, the authors have considered the constant vorticity of the shear current to be strong, as has also been confirmed by experimental observations (Steer et al., 2020). We proceed to derive a shear-current modified envelope equation based on the dispersion relation given by Equation 10a. The complex envelope A of the surface elevation is introduced such that

$$\zeta^{(1)} = \frac{1}{2}A(\mathbf{x},t)\mathrm{e}^{\mathrm{i}\psi_0} + \frac{1}{2}A^*(\mathbf{x},t)\mathrm{e}^{-\mathrm{i}\psi_0}, \text{ with } A(\mathbf{x},t) = \int \hat{A}(\mathbf{k},t)\mathrm{e}^{\mathrm{i}\mathbf{k}\cdot\mathbf{x}}\mathrm{d}\mathbf{k} \text{ and} \tag{12a}$$

$$\hat{A}(\mathbf{k},t) = 2\hat{\zeta}^{(1)}(\mathbf{k}+\mathbf{k}_0,0)\Theta((\mathbf{k}+\mathbf{k}_0)\cdot\mathbf{k}_0)\,\mathrm{e}^{-\mathrm{i}[\omega(\mathbf{k}+\mathbf{k}_0)-\omega_0]t}, \tag{12b}$$

where the asterisk denotes the complex conjugates, $\hat{A}(\mathbf{k},t)$ denotes the Fourier transform of the complex envelope A, Θ denotes the Heaviside step function, and $\psi_0 = (\mathbf{x}, t; \mathbf{k}_0, \omega_0)$ with $\omega_0 = \sqrt{gk_0}$ the angular frequency of the characteristic wave in the absence of a current by definition (Li, 2023). Using this definition of the complex envelope we obtain

$$\partial_t A = \int -\mathrm{i}\omega(\mathbf{k}+\mathbf{k}_0)\hat{A}(\mathbf{k},t)\mathrm{e}^{\mathrm{i}\mathbf{k}\cdot\mathbf{x}}\mathrm{d}\mathbf{k} + \mathrm{i}\omega_0 A. \tag{12c}$$

Inserting the approximate dispersion relation given by Equation 10a for $\omega(\mathbf{k}+\mathbf{k}_0)$ leads to

$$\omega(\mathbf{k}+\mathbf{k}_0) = \omega_0\left[\sqrt{\frac{|\mathbf{k}+\mathbf{k}_0|}{k_0}} + \frac{\tilde{U}_b(\mathbf{k}_0)}{\sqrt{g/k_0}} + \left(\sqrt{\frac{|\mathbf{k}+\mathbf{k}_0|}{k_0}}\ \frac{\tilde{U}_b(\mathbf{k}+\mathbf{k}_0)}{\sqrt{g/|\mathbf{k}+\mathbf{k}_0|}} - \frac{\tilde{U}_b(\mathbf{k}_0)}{\sqrt{g/k_0}}\right)\right]. \tag{13}$$

Let δ be the dimensionless bandwidth of surface waves, a leading-order approximation to $\omega(\mathbf{k}+\mathbf{k}_0) - \omega_0$ can be derived based on Equation 13

$$\omega(\mathbf{k}+\mathbf{k}_0) - \omega_0 \approx \omega_0\left(\sqrt{|\mathbf{k}+\mathbf{k}_0|/k_0} - 1 + \mathcal{U}(\mathbf{k}_0;\boldsymbol{\chi},\tau)\right) + \mathcal{O}(\mu_0\delta). \tag{14}$$

Following Li (2021) and Trulsen et al. (2000), we introduce the operator in the physical plane

$$\mathcal{L}(\partial_x,\partial_y) = \left[(1-\mathrm{i}\partial_x/k_0)^2 - \partial_y^2/k_0^2\right]^{1/4} - 1. \tag{15a}$$

Noting the operators in the physical and Fourier $\mathbf{k}$ plane, respectively, as follows

$$\nabla \to \mathrm{i}\mathbf{k} \text{ and } \mathcal{L}(\partial_x,\partial_y) \to \omega_0\mathcal{L}_\kappa = \sqrt{g|\mathbf{k}+\mathbf{k}_0|} - \sqrt{gk_0} \tag{15b}$$

where $\mathcal{L}_\kappa \equiv \mathcal{L}(\mathrm{i}k_x,\mathrm{i}k_y)$. Substituting the approximate form Equations 14 into 12c leads to

$$\partial_t A + \mathrm{i}\omega_0\mathcal{L}(\partial_x,\partial_y)A + \mathrm{i}\omega_0\mathcal{U}(\mathbf{k}_0;\boldsymbol{\chi},\tau)A = 0, \tag{16}$$

which is correct to $\max([\mathcal{O}(\varepsilon^2),\mathcal{O}(\mu_0\delta)])$. The linear envelope equation accounting for the effects of a shear current is given by Equation 16. In the absence of a background flow, we emphasize that the relation between

nonlinear wave evolution, Stokes drift, and low-vorticity waves has been discussed within the framework of the unidirectional NLS in A. Abrashkin and Pelinovsky (2017) and A. A. Abrashkin and Pelinovsky (2018).

2.2. The Higher-Order Shear-Current Wave Envelope Evolution Framework

Based on Equation 16 and following Dysthe (1979), we drive a Shear-Current Modified NLS (SC-MNLS) equation for the complex envelope A with the assumption that the order of magnitude of the background current velocity is at least at second-order in wave steepness, that is, $\mu_0 \sim \varepsilon^2$, which is mostly the case in the open-ocean. The assumption of the scales for the shear current means that the vertically sheared flow affects the evolution of the envelope in Equation 12c in $\mathcal{O}(\varepsilon^3)$. This leads to SC-MNLS equation for the complex envelope A by combing Equation 16 and the nonlinear terms in the NLS equation by Dysthe (1979) as follows (see Text S1.2 in Supporting Information S1 for detailed derivations)

$$\begin{aligned}\partial_t A + \mathrm{i}\omega_0 \mathcal{L}(\partial_x,\partial_y)A + 3k_0\omega_0|A|^2\partial_x A/2 + k_0\omega_0 A^2\partial_x A^*/4 \\ +\mathrm{i}A\omega_0\left[k_0^2|A|^2/2 + \partial_x\bar{\phi}(\mathbf{k},0,t)/(2c_{g,0}) + \mathcal{U}(\mathbf{k}_0;\boldsymbol{\chi},\tau)\right] = 0,\end{aligned} \tag{17}$$

where $c_{g,0}$ denotes the group propagation velocity of the wave packet in deep-water, $\bar{\phi}(\mathbf{x},z,t) = \omega_0 \int \mathrm{i}k_x \mathcal{F}\{|A|^2\}\exp(kz + \mathrm{i}\mathbf{k}\cdot\mathbf{x})/(2k)\mathrm{d}\mathbf{k}$ is the mean velocity potential at the second-order in wave steepness, with $\mathcal{F}$ representing the Fourier transform with respect to $\mathbf{x}$. While the first two terms in the square bracket of Equation 17 are the nonlinear terms in the famed Dysthe equation and accounting for the waves' directionality, the three terms in the square brackets of the same Equation 17 can be *physically* interpreted as the contribution of the Stokes drift, Eulerian return flow, and background flow as follows. A leading-order approximation to the Stokes drift velocity is given by Longuet-Higgins (1953), van den Bremer et al. (2019), and Li and Li (2021):

$$U_s(\mathbf{x},z,t) = 2c_{g,0}(k_0|A|)^2\exp(2k_0 z). \tag{18}$$

We introduce a wavenumber-weighted and depth-integrated velocity $\tilde{U}_s$, defined by integrating the product of the carrier wavenumber and the Stokes drift velocity over the entire water column

$$\tilde{U}_s(A) = \int_{-\infty}^{0} k_0 U_s(\mathbf{x},z,t)\mathrm{d}z \text{ such that } \tilde{U}_s(A) = c_{g,0}(k_0|A|)^2. \tag{19}$$

Similarly, we introduce a physical velocity due to the Eulerian return flow defined as

$$\tilde{U}_e(A) \equiv \partial_x\bar{\phi}(\mathbf{x},0,t) = -c_{g,0}\int\left[k_x^2/(kk_0)\right]\mathcal{F}\{k_0^2|A|^2\}\,\mathrm{e}^{\mathrm{i}\mathbf{k}\cdot\mathbf{x}}\mathrm{d}\mathbf{k}. \tag{20}$$

The negative sign in Equation 20 is due to the flow propagating opposing to the main propagation direction of the wavepacket. Inserting Equation 19 for $k_0^2|A|^2$, Equation 20, and the definition of $\mathcal{U}$ according to Equation 11 into the SC-MNLS

$$\partial_t A + \mathrm{i}\omega_0\mathcal{L}(\partial_x,\partial_y)A + \left(\frac{3k_0\omega_0}{2}|A|^2\partial_x A + \frac{k_0\omega_0}{4}A^2\partial_x A^*\right) + \mathrm{i}A\omega_0\frac{\tilde{U}_s + \tilde{U}_e + \tilde{U}_b}{2c_{g,0}} = 0, \tag{21}$$

where the subscripts "s,", "e," and "b" denotes the contribution due to the Stokes drift, Eulerian return flow, and background flow, respectively, at leading order of $\mathcal{O}(\varepsilon^2)$, $\mathcal{O}(\varepsilon^2\delta)$, and $\mathcal{O}(\mu_0)$, the first two terms and these in the big round brackets are at $\mathcal{O}(\varepsilon\delta)$ and $\mathcal{O}(\varepsilon^3\delta)$, respectively. The updated SC-MNLS equation described by Equation 21 shows, mathematically, how the interplay of the Stokes drift, Eulerian return flow, and background flow affects the evolution of the complex wave envelope. The physical interpretations of Equation 21 in the modulational instability of Stokes waves are elucidated next in Section 3.1.

We remark that, with additional assumptions, Equation 21 can be used to recover different previous versions of dynamic evolution equations for the envelope. For example, without a background flow where $\widetilde{\mathbf{U}}_b = 0$,

Equation 21 recovers to the modified NLS equation derived by Trulsen et al. (2000, their Equation 19). With the narrowband assumption of $\delta \ll 1$, the operator $\mathcal{L}$ admits a leading-order approximation

$$\mathcal{L}(\partial_x,\partial_y) = -\mathrm{i}\partial_x/(2k_0) + (\partial_{xx} - 2\partial_{yy})/\left(8k_0^2\right) + \mathrm{i}(\partial_{xxx} - 6\partial_{xyy})/\left(16k_0^3\right), \tag{22}$$

which is truncated to $\mathcal{O}\left(\delta^3\right)$. A lower-order approximation to $\mathcal{L}$ can be obtained based on Equation 22. More specifically, removing the terms in $\mathcal{O}\left(\delta^2\right)$ ($\mathcal{O}\left(\delta^3\right)$) and higher leads to a first-order (second-order) approximation. Substituting the first-order approximation to $\mathcal{L}$ into the SC-MNLS equation, eliminating the nonlinear terms in the big round brackets, and neglecting the effects of the Eulerian return flow, that is, $\tilde{U}_e = 0$, recovers the wave envelope dynamic equation by McWilliams et al. (2004, their Equation 5.35) in the limit of infinite water depth. Similarly, using the second-order approximation for $\mathcal{L}$ instead and with the neglected nonlinear terms in the round brackets, negligible y dependence, and vanishing Eulerian return flow, Equation 21 leads to the equation in a similar structure as that derived by Pizzo et al. (2023, their Equation 3.16) for long-crested waves in a Lagrangian frame.

3. Results and Discussion

3.1. Influence of Shear-Currents on the Modulational Instability

Based on Equation 21 a uniform wave solution with a constant amplitude a_0 is given by

$$A = a_0 \exp\left[-\mathrm{i}\omega_0 t\left(\tilde{U}_s(a_0) + \tilde{U}_b\right)/(2c_{g,0})\right]. \tag{23}$$

The stability of the uniform wave to sideband perturbations is investigated assuming small perturbations in amplitude a and phase θ of the form

$$A = a_0(1 + a + \mathrm{i}\theta)\exp\left[-\mathrm{i}\omega_0 t\left(\tilde{U}_s(a_0) + \tilde{U}_b\right)/(2c_{g,0})\right] \tag{24}$$

having the plane wave solution $[a,\theta] = \left[\hat{a},\hat{\theta}\right]\exp\left[\mathrm{i}(\delta_x k_0 x + \delta_y k_0\, y - \delta_\omega \omega_0 t)\right] + \text{c.c.}$, where c.c. denotes the complex conjugates, δ_x and δ_y denote the (real) dimensionless bandwidth in the longitudinal and transverse direction, respectively, and δ_ω the dimensionless bandwidth in wave frequency, $\hat{a}$ and $\hat{\theta}$ denote the (real) amplitude and phase of the perturbations which are assumed to be small compared with the amplitude a_0 of the uniform wave. Inserting Equation 24 for the envelope into Equation 21 leads to a linearized perturbation equation whose solution gives rise to an expression for the dimensionless frequency, δ_ω. The expression depends on the velocity profile of the background flow.

As noted, a background flow in ocean models with surface waves being a driving force shall have a component called *wave-modified background flow*. This suggests that such a flow in addition depends on the perturbations. We may assume the velocity profile of the wave-modified background flow in the form (see, e.g., Pizzo et al. (2023); Higgins et al. (2020))

$$\tilde{U}_b \equiv \tilde{U}_b(A) \sim c_{g,0}\left(k_0^2|A|^2\right), \text{ and thus } \tilde{U}_b/c_{g,0} \sim \mu_0 \sim \varepsilon^2 \text{ as assumed.} \tag{25a, b}$$

Due to Equation 25, inserting the envelope given by Equation 24 into the SC-MNLS, the linearized perturbation equation leads to an explicit expression for the dimensionless frequency δ_w,

$$\delta_\omega = \mathcal{L}_i \pm \sqrt{\Delta} \text{ with } \Delta = \mathcal{L}_r\left[\mathcal{L}_r + \epsilon_0{}^2\left(\gamma_s + \gamma_e + \gamma_b\right)\right] + \delta_x^2\epsilon_0{}^4/16, \tag{26a, b}$$

where $\epsilon_0 = k_0 a_0$ is the wave steepness, $\mathcal{L}_i = [\mathcal{L}(\mathrm{i}\delta_x k_0,\mathrm{i}\delta_y k_0) + \mathcal{L}^*(\mathrm{i}\delta_x k_0,\mathrm{i}\delta_y k_0)]/2$ and $\mathcal{L}_r = -\mathrm{i}[\mathcal{L}(\mathrm{i}\delta_x k_0,\mathrm{i}\delta_y k_0) - \mathcal{L}^*(\mathrm{i}\delta_x k_0,\mathrm{i}\delta_y k_0)]/2$, and the other non-dimensional parameters γ with different subscripts are given by

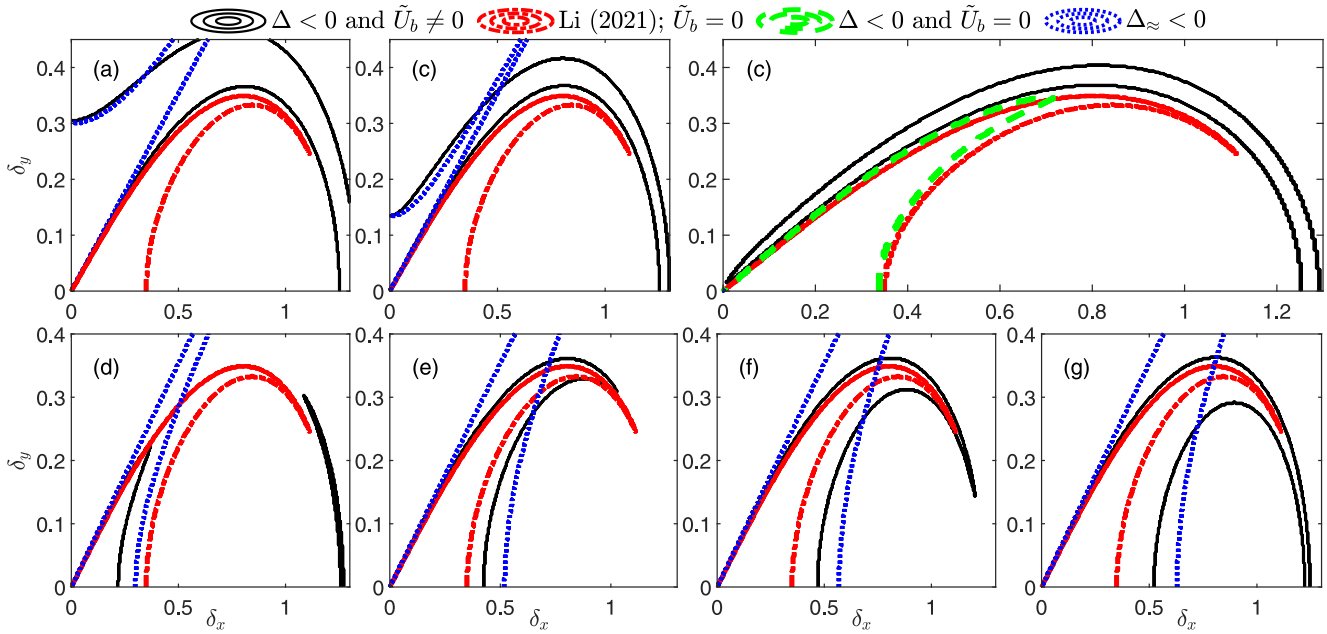

Figure 1. The instability region against the sidebands δ_x and δ_y in the main direction of the carrier wave propagation and the transverse direction, respectively, where $\epsilon_0 = 0.15$. The panels (a–g) are obtained based on (26b) (back solid) with an increasing γ_b, from the negative value of $-2, -1.2, -1, -0.5$ denoting an opposing current to the positive value of 0.5, 0.8, and 1.2 which denotes a background flow following the carrier wave. In all panels, the instability region in the absence of a background current predicted by Li (2021) (red dashed) and the approximation $\Delta_{\approx}$ (blue dots) are included.

$$\gamma_s \equiv \frac{1}{{\epsilon_0}^2}\frac{\tilde{U}_s(a_0)}{c_{g,0}} = 1, \gamma_e = \frac{1}{{\epsilon_0}^2}\frac{\tilde{U}_e(k_0,a_0,0)}{c_{g,0}}, \text{ and } \gamma_b = \frac{1}{{\epsilon_0}^2}\frac{\tilde{U}_b(a_0)}{c_{g,0}} \tag{27a, b, c}$$

which are interpreted as the effect of the Stokes drift, Eulerian return flow, and the perturbed background flow on the stability of a uniform wave, respectively. The sideband instability occurs when the imaginary component of the dimensionless frequency δ_w is positive, requiring the inequality

$$\Delta < 0 \tag{28}$$

to hold. This inequality defines a region of instability shown in Figure 1. The region of instability varying with the longitudinal (δ_x) and transverse bandwidth (δ_y) is computed in Figure 1 with an increasing value for γ_{ba} for the panels from (a) to (f).

Figure 1 shows consistent results with the following discussions using the approximation $\mathcal{L}_r \approx \delta_y^2/4 - \delta_x^2/8$. When neglecting, in addition, the effects due to Eulerian return flow and the nonlinear terms dependent on the bandwidth, the inequality $\Delta < 0$, as in Equation 28, becomes

$$\Delta_{\approx} < 0 \text{ with } \Delta_{\approx} \equiv \left(\delta_y^2/4 - \delta_x^2/8\right)\left[\delta_y^2/4 - \delta_x^2/8 + {\epsilon_0}^2\left(\gamma_s + \gamma_b\right)\right]. \tag{29a, b}$$

The inequality Equation 29b recovers to Pizzo et al. (2023, their Equation 3.18) in the limiting cases of long-crested waves where $\delta_y = 0$, albeit it shall be noted that the theory by Pizzo et al. (2023) is derived in a Lagrangian frame. Based on Equation 26b, the suppression of the MI occurs if $\Delta = 0$ as this means the perturbations cannot grow. In the limit of extremely small waves where $\epsilon_0 \to 0$, the identity $\Delta = 0$ is met under two conditions

$$\gamma_s + \gamma_e + \gamma_b = 0, \tag{30}$$

which means $\Delta = 0$ when $\mathcal{L}_r = 0$ and $\Delta = \mathcal{L}_r^2 \geq 0$ in general, or

$$\gamma_s + \gamma_e + \gamma_b = \left(\delta_x^2 - 2\delta_y^2\right)/\left(8{\epsilon_0}^2\right). \tag{31}$$

The identities Equations 30 and 31 define the boundaries of the region where the MI occurs, as a result of the interplay of the three different flows. Given that $\gamma_s = 1$ based on Equation 27a and $\gamma_e \to 0^-$ as $\varepsilon \to 0$ based on Equation 27b, the identities Equations 30 and 31 holds when

$$\gamma_b \approx -1 \text{ and } \gamma_b \approx \left(\delta_x^2 - 2\delta_y^2\right)/\left(8{\epsilon_0}^2\right) - 1, \tag{32a, b}$$

respectively. The identity Equation 32a corresponds to the case of an opposing current. The ratio of bandwidth to steepness in Equation 32b has the same sign as the sign of $\gamma_b + 1$, meaning an opposing current with $\gamma_b < -1$ leads to the region boundaries of the MI intersect with the axis of the transverse bandwidth at $\delta_y \approx 2\epsilon_0\sqrt{-1-\gamma_b}$ or with the positive axis of the longitudinal bandwidth at $\delta_x \approx 2\,\epsilon_0\sqrt{2\left(1+\gamma_b\right)}$ for $\gamma_b > -1$.

With the definition of γ_b given by Equation 27c, the approximation $\gamma_b \approx -1$ based on Equation 32a is a special case that has a twofold meaning, as shown in panel (c) of Figure 1. Firstly, the instability for long-crested waves starts to be completely suppressed if the magnitude of the flow becomes stronger. Secondly, it leads to an extremely limited instability region near the origin as inserting the approximation into Equation 32b leads to $\delta_x = \delta_y = 0$. This special case corresponds to an estimate of the magnitude of the background flow

$$\tilde{U}_b/c_{g,0} \sim -{\epsilon_0}^2, \tag{33}$$

which falls into the regime of a background flow that predominantly occurs in the open ocean, especially, the wind-drift currents (Leibovich, 1983; J. Wu, 1983). For example, when wind waves have a typical spectral peak period of 10 s, which corresponds to the phase velocity of ∼16 m/s, the suppression of the MI occurs for $\tilde{U}_b \approx -0.18$ m/s and $\tilde{U}_b \approx 0.08$ m/s and $\epsilon_0 = 0.15$, corresponding to wind-drift currents whose velocity on a still water surface ($|\mathbf{U}_b(z=0)|$) of ∼2.25% and ∼1% of the wind speed, respectively.

The condition for the suppression of MI of long-crested waves also corresponds to when the transverse instability starts to be more pronounced with $\gamma_b \le -1$, as shown in panels (a–c) in Figure 1. When the longitudinal bandwidth vanishes, that is, $\delta_x = 0$, Equation 26b has two roots for the dimensionless transverse bandwidth δ_y

$$\delta_y = 0 \text{ or } \delta_y \approx 2\epsilon_0\sqrt{-\left(\gamma_s + \gamma_b + \gamma_e\right)}. \tag{34a, b}$$

Substituting the values for γ_b of −2, −1.2, and −1 into Equation 34b leads to the value for the dimensionless transverse bandwidth of ∼0.30, 0.13, and 0, respectively. This is in agreement with the graphic intersection of the boundary of the instability region (black solid lines) with the vertical axis in panel (a), (b), and (c) of Figure 1, respectively. This can also be observed in Figure 2 in which a slightly higher value for the wave steepness was adopted. Figure 2 shows that the MI for unidirectional or long-crested waves is suppressed for $\gamma_b \le -1$. When the instability occurs, $|\sqrt{\Delta}|$ (or $|\sqrt{\Delta_{\approx}}|$) quantifies the growth rate of the energy transfers. The Eulerian return flow represented by γ_e, with $0 \le \gamma_e < 1$, leads especially to a decreased growth rate and has larger effects on the decreased growth rate for larger longitudinal bandwidth or steepness.

The estimate of the background flow modified constant, γ_b, depends on the vertical profile in addition to the order of magnitude of the velocity of the background flow given by Equation 25. We may express the velocity component of the background flow as

$$U_{k_0} = 2c_{g,0}k_0^2|A|^2\bar{U}(z), \tag{35}$$

where the subscript "k_0" denotes the projection of the velocity vector $\mathbf{U}_b$ in the main propagation direction of the waves, $\mathbf{k}_0$; $\bar{U}(z) \sim \mathcal{O}(1)$ denotes a dimensionless function that shows the dependence of the velocity on depth z. We consider three different profiles which can lead to an explicit expression for γ_b

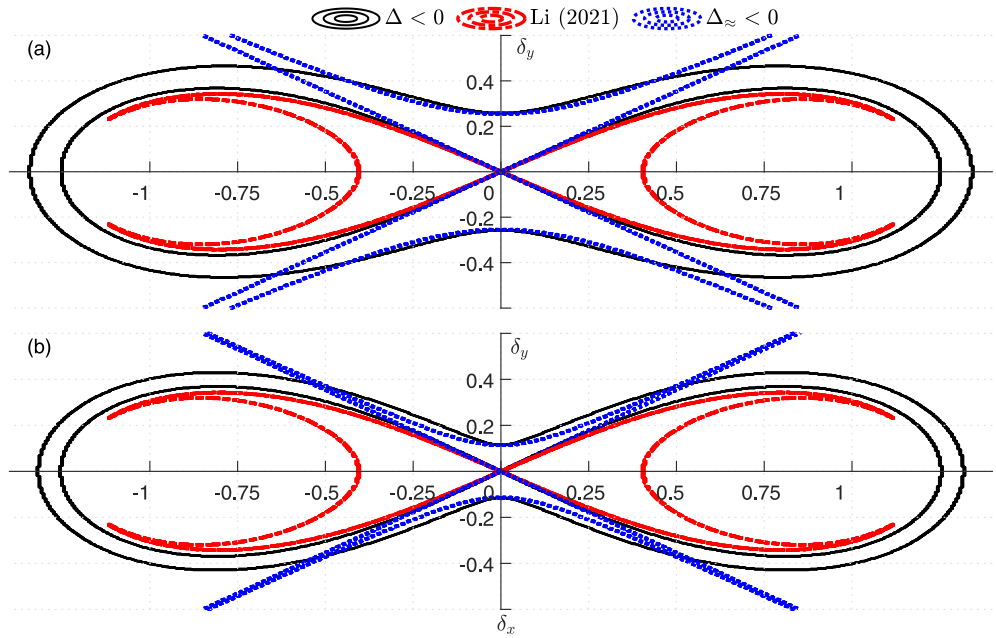

Figure 2. Instability region similarly to Figure 1. In panels (a, b) $\epsilon_0 = 0.18$ with different values for γ_b: panel (a) $\gamma_b = -1.5$ and panel (b) $\gamma_b = -1.1$.

$$\bar{U}(z) \equiv \bar{U}_c = \bar{U}_0 \;\rightarrow\; \gamma_b = 2\bar{U}_0, \tag{36a}$$

$$\bar{U}(z) \equiv \bar{U}_{\exp} = \bar{U}_0(\exp(\Lambda k_0 z) - \upsilon) \;\rightarrow\; \gamma_b = 2U_0\left[2(2+\Lambda)^{-1} - \upsilon\right], \tag{36b}$$

$$\bar{U}(z) \equiv \bar{U}_L = U_0 + Sk_0 z \;\rightarrow\; \gamma_b = 2U_0(1 - S/2), \tag{36c}$$

where the subscripts "c," "exp," and "L" denote a constant, exponential, and linear profile, respectively; $\bar{U}_0 = \bar{U}(0)$ is the dimensionless velocity at the still water surface; Λ, υ, and S are dimensionless parameters that are chosen to denote the different dependence of the profile of the vertical shear current on z. In the limiting case of $\gamma_b = -1$ which corresponds to suppressed MI in wave dynamics, Equations 36a–36c lead to, respectively,

$$\bar{U}_0 = -1/2, \;\; -1 = \bar{U}_0[4/(2+\Lambda) - 2\upsilon], \text{ and } \; -1 = \bar{U}_0(1 - S/2). \tag{37a, b, c}$$

In the presence of the exponential sheared current for $\upsilon = 0$, $\Lambda = 2$, and $\bar{U}_0 = -1$ such that

$$U_{k_0} = -2c_{g,0}k_0 e^{2k_0 z}(k_0|A|)^2 \equiv -U_s(z), \tag{38}$$

it particularly represents a case of suppressed MI, when the Stokes drift velocity is canceled out by the background flow at different depths.

We emphasize that when a shear current is not considered correlated to the waves, that is, the current is only interpreted as a Doppler shift to the frequency (see, e.g., Cavaleri et al. (2018)), $\gamma_b = 0$ is admitted and the shear currents with the assumed scales discussed in this section do not affect the MI process.

3.2. Impact of the Background Flow and Modulational Instability on Langmuir Circulations

We have so far demonstrated how a system of surface waves in a sheared mean flow becomes unstable subject to small perturbations owing to MI. It is interesting to point out that this system can also be unstable to small spanwise perturbations arising from the CL2 instability mechanism, which leads to vertical vortex lines being tilted, the generation of streamwise vorticity, and enhanced vertical motions (Thorpe, 2004). Likely due to the applications in two different communities, that is, wave hydrodynamics and ocean modeling, we remark that both

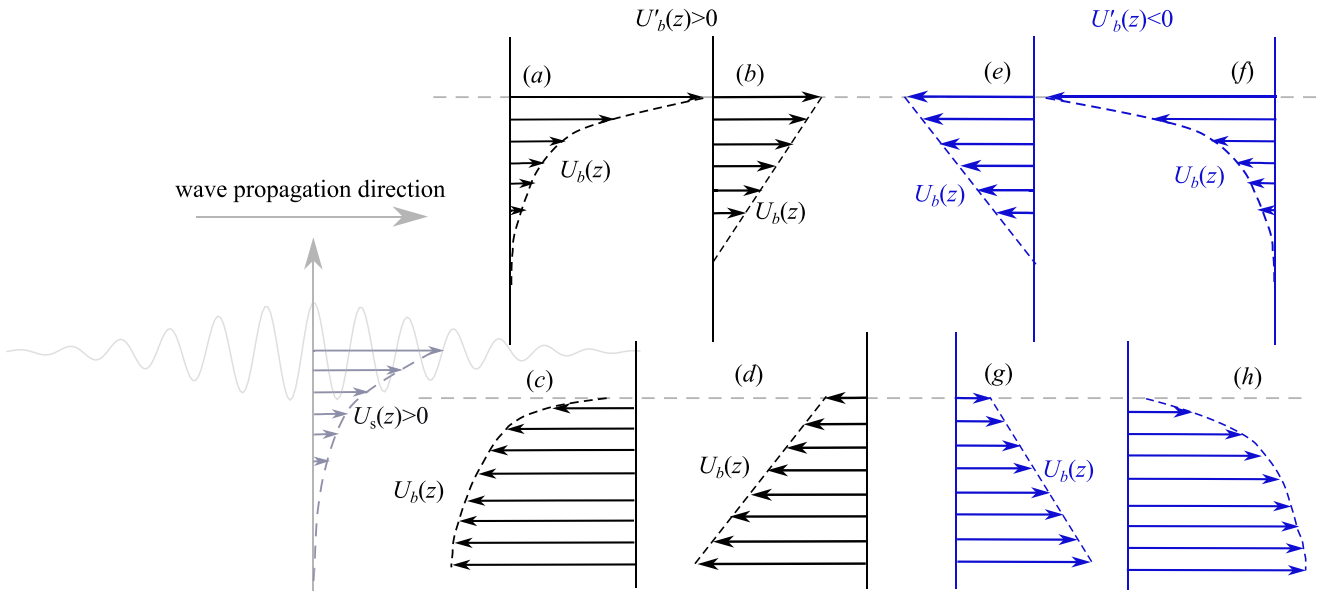

Figure 3. Diagram of the profiles of a background flow with monotonically varying velocities with depth. In the Figure, $U_s(z)$ denotes the velocity of the Stokes profile beneath a train of right-propagating quasi-monochromatic waves; $U_b(z)$ denotes the component profile of a horizontally uniform and vertically sheared flow in the direction of wave propagation. Panels (a–d) and (e–h) show a profile of a sheared current which can and cannot lead to the CL2 instability, respectively. Panels (a, b, g, h) and (c–f) show a profile of vertically sheared current which can enhance and suppress the MI of long-crested waves.

instability mechanisms have been separately considered in the past. Whether the two different phenomena of great interest to the different communities shall be considered together is an open research question that requires further studies. Nevertheless, it can be instructive to point out the conditions which can establish a possible relationship between the two mechanisms. Specifically, the conditions correspond to when both instabilities can occur or when one occurs, however, the other is instead suppressed.

Following Craik and Leibovich (1976) and Leibovich (1977, 1983), the linearized stability analysis can be applied for the mean flows denoted by $\boldsymbol{\mathcal{U}}$ here, while detailed derivations are not included to avoid unnecessary repetition. The same conclusions can be drawn to determine the condition for which the CL2 instability occurs

$$U'_b U'_s > 0, \tag{39}$$

which applies for inviscid and non-stratified shear flows with negligible Earth's rotation. We recall that U'_b and U'_s are the vertical gradients of the shear current and Stokes drift, respectively, as in Leibovich (1983). The timescale for the modulational and CL2 instability to occur is, respectively

$$\left(\omega_0 \epsilon^2\right) t_w \sim 1 \text{ and } 0.2\omega_0 \epsilon t_c \sim 1, \tag{40a, b}$$

the latter of which is estimated using the properties of the mean flow as follows. The mean flow is assumed to be a wind-drift current of the order of 3% of the wind speed (Leibovich, 1977, their Section 6). The timescales of the two different mechanisms for an unstable system estimated by Equations 40a, b mean that these are of the same order, and thus nonlinear energy transfers between waves and between waves and currents are expected to occur in the ocean within the same time duration. This is indeed a feature that should be useful from an observational point of view.

Combing the discussion in Section 3.1 and the criterion by Equation 39 for the modulational and CL2 instability, respectively, both mechanisms depend on the profile of Stokes drift and vertically sheared current. To demonstrate this, a diagram of a train of right-propagating quasi-monochromatic waves in a vertically sheared current modeled by different velocity profiles is shown in Figure 3. We stress that the discussion here is not limited to the current profiles whose magnitude varies monotonically with depth, although they are used as examples in Figure 3. The profiles shown by panels (a, b) and (e, f), which are typical as wind-drift currents (Peregrine, 1976),

can trigger and suppress both instabilities, respectively, as the profiles in panels (a, b) can satisfy Equation 39 and a following current leads to an increased area of the region of the MI of long-crested waves, while the profiles in panels (e, f) suppresses the streamwise MI instability of long-crested waves and the CL2 instability. The profiles by panels (c, d) and (g, h) can be used to model the superposition of a tidal current and a wind-drift current. Panels (c, d) show that the CL2 can be triggered but suppress the MI due to transverse perturbations, whereas panels (g, h) show the opposite phenomena. The profiles depicted by panels (c, d) can be unstable to oblique perturbations due to the additional MI to the CL2 instability, similar to panels (a, b). Note that Gerstner waves do not induce drift and thus, neither Langmuir circulation (Holm, 1996; A. A. Abrashkin & Pelinovsky, 2018).

4. Conclusion

Using a newly derived shear-current modified NLS equation for narrowband deep-water surface waves in a background open flow, we have explicitly represented the roles of three different currents in the generation of extremely large amplitude sea waves subject to MI in three dimensions. These three different currents are a Stokes drift, an Eulerian return flow due to a passing quasi-monochromatic wave group, and an open-ocean background flow with induced motions being also rotational. The background flow is assumed to be horizontally oriented but vertically sheared, whose velocity varies slowly in the horizontal space and time compared with the phase of the characteristic wave. The magnitude of the background flow has a component at the second order in wave steepness in the main propagation direction of waves.

The complex interplay between the three flows is represented by the superposition of three dimensionless parameters in the shear SC-MNLS equation, which is used in the condition given by Section 3.1 for the MI to occur. When the background flow is simply interpreted as a Doppler shift being completely uncorrelated with external perturbations and waves, it does not affect the conditions for the occurrence of MI. Nevertheless, for the opposite case, that is, the background flow is both perturbation and waves correlated (Pizzo et al., 2023), its role is interpreted by the dimensionless parameter γ_b defined in Equation 27c, denoting the magnitude of the shear current-modified effect scaled with the product of ${\epsilon_0}^2$ and $c_{g,0}$, where ϵ_0 and $c_{g,0}$ denotes the dimensionless steepness and group velocity of the carrier wave, respectively. It is worth noting that the effect of the vertically sheared current is depth-averaged as well as wave vector-weighted, which means the effect on waves depends on both, wavelength and the angle between wave propagation and current orientation (Ellingsen & Li, 2017). An opposing and following flow can, in general, suppress or enhance the MI of unidirectional (long-crested) waves. The MI of such waves can be completely suppressed when $\gamma_b \leq -1$, whereas the oblique instability remains not affected. The conditions of $\gamma_b \leq -1$ can be found especially in wind-drift currents as their magnitude is about the order of ${\epsilon_0}^2$ of the characteristic wind speed, which can be well-approximated by the phase velocity of local wind-induced waves (Leibovich, 1983; J. Wu, 1983).

The Stokes drift is explicitly represented by $\tilde{U}_s$ in Equation 19 in the newly derived NLS-type equation given by Equation 21 in an Eulerian frame. It has been widely used in wave-induced mean flow equations for understanding the dynamics of the upper ocean flow, partly due to its role in triggering the CL2 instability which can tilt and generate vortex rolls and promote vertical motions in the upper ocean (see, e.g., Suzuki and Fox-Kemper (2016)). Both the MI and CL2 instability can lead to a system composed of surface waves and an open-ocean flow becoming unstable subject to small perturbations. We have determined combined conditions for the occurrence of both, therefore demonstrated that these processes shall be considered together to determine energy transfers between waves and between wave and current interactions in realistic circumstances in the open ocean.

Although the reported findings are based on asymptotic approximate theory, they can be used to guide and better interpret in situ observations (Malila et al., 2023). Moreover, the roles of a background flow on the MI have demonstrated the need for physically coupling the ocean and wave models in the upper mixed ocean layer, in which the wave phases should be resolved. In doing so, when both instabilities occur in the open ocean, energy cascades from waves to waves to currents and vice versa may open up novel physical insights in the perspective of the partition of the energy of surface waves in the real ocean, as studied in S. F. Zippel et al. (2022), and the maintenance of Langmuir circulations by surface waves (Phillips, 2002; Thorpe, 2004). Furthermore and similarly to the Dysthe equation (Kit & Shemer, 2002; Lo & Mei, 1985; Pizzo & Melville, 2016; Trulsen & Stansberg, 2001), a spatial form of our newly derived framework can be useful for experimental explorations and numerical benchmark studies to assess the influence of an additional mean flow on the evolution of nonlinear waves.

Data Availability Statement

All figures and data from this work can be reproduced by following the theoretical equations used.

Acknowledgments
YL acknowledges the support from the Research Council of Norway through a POS-ERC Grant (project no. 342480). AC is supported by the Hakubi Center for Advanced Research at Kyoto University.

References

Abrashkin, A., & Pelinovsky, E. (2017). Lagrange form of the nonlinear Schrödinger equation for low-vorticity waves in deep water. *Nonlinear Processes in Geophysics*, *24*(2), 255–264. https://doi.org/10.5194/npg-24-255-2017

Abrashkin, A. A., & Pelinovsky, E. N. (2018). On the relation between Stokes drift and the Gerstner wave. *Physics-Uspekhi*, *61*(3), 307–312. https://doi.org/10.3367/ufne.2017.03.038089

Ardhuin, F., Rascle, N., & Belibassakis, K. A. (2008). Explicit wave-averaged primitive equations using a generalized Lagrangian mean. *Ocean Modelling*, *20*(1), 35–60. https://doi.org/10.1016/j.ocemod.2007.07.001

Babanin, A. V., & Chalikov, D. (2012). Numerical investigation of turbulence generation in non-breaking potential waves. *Journal of Geophysical Research*, *117*(C11). https://doi.org/10.1029/2012jc007929

Banihashemi, S., & Kirby, J. T. (2019). Approximation of wave action conservation in vertically sheared mean flows. *Ocean Modelling*, *143*, 101460. https://doi.org/10.1016/j.ocemod.2019.101460

Benjamin, T. B. (1967). Instability of periodic wavetrains in nonlinear dispersive systems. *Proceedings of the Royal Society of London. Series A, Mathematical and Physical Sciences*, *299*(1456), 59–76.

Breivik, Ø., Bidlot, J., & Janssen, P. (2016). A Stokes drift approximation based on the Phillips spectrum. *Ocean Modelling*, *100*, 49–56. https://doi.org/10.1016/j.ocemod.2016.01.005

Breivik, Ø., & Christensen, K. H. (2020). A combined Stokes drift profile under swell and wind sea. *Journal of Physical Oceanography*, *50*(10), 2819–2833. https://doi.org/10.1175/jpo-d-20-0087.1

Breivik, Ø., Janssen, P. A. E. M., & Bidlot, J. R. (2014). Approximate Stokes drift profiles in deep water. *Journal of Physical Oceanography*, *44*(9), 2433–2445. https://doi.org/10.1175/jpo-d-14-0020.1

Cavaleri, L., Abdalla, S., Benetazzo, A., Bertotti, L., Bidlot, J.-R., Breivik, Ø., et al. (2018). Wave modelling in coastal and inner seas. *Progress in Oceanography*, *167*, 164–233. https://doi.org/10.1016/j.pocean.2018.03.010

Chabchoub, A., Hoffmann, N., & Akhmediev, N. (2011). Rogue wave observation in a water wave tank. *Physical Review Letters*, *106*(20), 204502. https://doi.org/10.1103/physrevlett.106.204502

Craik, A., & Leibovich, S. (1976). A rational model for Langmuir circulations. *Journal of Fluid Mechanics*, *73*(3), 401–426. https://doi.org/10.1017/s0022112076001420

D'Asaro, E. A. (2014). Turbulence in the upper-ocean mixed layer. *Annual Review of Marine Science*, *6*(1), 101–115. https://doi.org/10.1146/annurev-marine-010213-135138

Dudley, J. M., Genty, G., Mussot, A., Chabchoub, A., & Dias, F. (2019). Rogue waves and analogies in optics and oceanography. *Nature Reviews Physics*, *1*(11), 675–689. https://doi.org/10.1038/s42254-019-0100-0

Dysthe, K. (1979). Note on a modification to the nonlinear Schrödinger equation for application to deep water waves. *Proceedings of the Royal Society of London A.*, *369*(1736), 105–114.

Ellingsen, S. A., & Li, Y. (2017). Approximate dispersion relations for waves on arbitrary shear flows. *Journal of Geophysical Research: Oceans*, *122*(12), 9889–9905. https://doi.org/10.1002/2017jc012994

Fujimoto, W., Waseda, T., & Webb, A. (2019). Impact of the four-wave quasi-resonance on freak wave shapes in the ocean. *Ocean Dynamics*, *69*(1), 101–121. https://doi.org/10.1007/s10236-018-1234-9

Guimarães, P. V., Ardhuin, F., Bergamasco, F., Leckler, F., Filipot, J., Shim, J., et al. (2020). A data set of sea surface stereo images to resolve space-time wave fields. *Scientific Data*, *7*(1), 145. https://doi.org/10.1038/s41597-020-0492-9

Higgins, C., van Den Bremer, T., & Vanneste, J. (2020). Lagrangian transport by deep-water surface gravity wavepackets: Effects of directional spreading and stratification. *Journal of Fluid Mechanics*, *883*, A42. https://doi.org/10.1017/jfm.2019.877

Hjelmervik, K. B., & Trulsen, K. (2009). Freak wave statistics on collinear currents. *Journal of Fluid Mechanics*, *637*, 267–284. https://doi.org/10.1017/s0022112009990607

Holm, D. D. (1996). The ideal Craik-Leibovich equations. *Physica D: Nonlinear Phenomena*, *98*(2–4), 415–441. https://doi.org/10.1016/0167-2789(96)00105-4

Janssen, P. A. (2003). Nonlinear four-wave interactions and freak waves. *Journal of Physical Oceanography*, *33*(4), 863–884. https://doi.org/10.1175/1520-0485(2003)33<863:nfiafw>2.0.co;2

Janssen, P. A., & Bidlot, J.-R. (2018). Progress in operational wave forecasting. *Procedia IUTAM*, *26*, 14–29. https://doi.org/10.1016/j.piutam.2018.03.003

Kharif, C., & Pelinovsky, E. (2003). Physical mechanisms of the rogue wave phenomenon. *European Journal of Mechanics - B: Fluids*, *22*(6), 603–634. https://doi.org/10.1016/j.euromechflu.2003.09.002

Kirby, J. T., & Chen, T. M. (1989). Surface waves on vertically sheared flows: Approximate dispersion relations. *Journal of Geophysical Research*, *94*(C1), 1013–1027. https://doi.org/10.1029/jc094ic01p01013

Kit, E., & Shemer, L. (2002). Spatial versions of the Zakharov and Dysthe evolution equations for deep-water gravity waves. *Journal of Fluid Mechanics*, *450*, 201–205. https://doi.org/10.1017/s0022112001006498

Lane, E. M., Restrepo, J., & McWilliams, J. C. (2007). Wave–current interaction: A comparison of radiation-stress and vortex-force representations. *Journal of Physical Oceanography*, *37*(5), 1122–1141. https://doi.org/10.1175/jpo3043.1

Lavrenov, I. (1998). The wave energy concentration at the agulhas current off South Africa. *Natural Hazards*, *17*(2), 117–127. https://doi.org/10.1023/a:1007978326982

Leibovich, S. (1977). Convective instability of stably stratified water in the ocean. *Journal of Fluid Mechanics*, *82*(3), 561–581. https://doi.org/10.1017/s0022112077000846

Leibovich, S. (1983). The form and dynamics of Langmuir circulations. *Annual Review of Fluid Mechanics*, *15*(1), 391–427. https://doi.org/10.1146/annurev.fl.15.010183.002135

Li, Y. (2021). Three-dimensional surface gravity waves of a broad bandwidth on deep water. *Journal of Fluid Mechanics*, *926*, 1–43. https://doi.org/10.1017/jfm.2021.711

Li, Y. (2023). On coupled envelope evolution equations in the Hamiltonian theory of nonlinear surface gravity waves. *Journal of Fluid Mechanics*, *960*, A33. https://doi.org/10.1017/jfm.2023.205

Li, Y., & Ellingsen, S. Å. (2019). A framework for modeling linear surface waves on shear currents in slowly varying waters. *Journal of Geophysical Research: Oceans*, *124*(4), 2527–2545. https://doi.org/10.1029/2018JC014390
Li, Y., & Li, X. (2021). Weakly nonlinear broadband and multi-directional surface waves on an arbitrary depth: A framework, Stokes drift, and particle trajectories. *Physics of Fluids*, *33*(7), 076609. https://doi.org/10.1063/5.0057215
Lo, E., & Mei, C. C. (1985). A numerical study of water-wave modulation based on a higher-order nonlinear Schrödinger equation. *Journal of Fluid Mechanics*, *150*, 395–416. https://doi.org/10.1017/s0022112085000180
Longuet-Higgins, M. S. (1953). Mass transport in water waves. *Philosophical Transactions of the Royal Society A*, *245*(903), 535–581.
Longuet-Higgins, M. S., & Stewart, R. (1962). Radiation stress and mass transport in gravity waves, with application to 'surf beats. *Journal of Fluid Mechanics*, *13*(4), 481–504. https://doi.org/10.1017/s0022112062000877
Madec, G., Bourdallé-Badie, R., Bouttier, P., Bricaud, C., Bruciaferri, D., Calvert, D., et al. (2017). Nemo ocean engine.
Malila, M. P., Barbariol, F., Benetazzo, A., Breivik, Ø., Magnusson, A. K., Thomson, J., & Ward, B. (2023). Statistical and dynamical characteristics of extreme wave crests assessed with field measurements from the North Sea. *Journal of Physical Oceanography*, *53*(2), 509–531. https://doi.org/10.1175/jpo-d-22-0125.1
McIntyre, M. (1981). On the "wave momentum" myth. *Journal of Fluid Mechanics*, *106*(-1), 331–347. https://doi.org/10.1017/s0022112081001626
McWilliams, J. C. (2016). Submesoscale currents in the ocean. *Proceedings of the Royal Society of London A.*, *472*(2189), 20160117. https://doi.org/10.1098/rspa.2016.0117
McWilliams, J. C., Restrepo, J. M., & Lane, E. M. (2004). An asymptotic theory for the interaction of waves and currents in coastal waters. *Journal of Fluid Mechanics*, *511*, 135–178. https://doi.org/10.1017/s0022112004009358
Mellor, G. (2015). A combined derivation of the integrated and vertically resolved, coupled wave–current equations. *Journal of Physical Oceanography*, *45*(6), 1453–1463. https://doi.org/10.1175/jpo-d-14-0112.1
Mellor, G. (2016). On theories dealing with the interaction of surface waves and ocean circulation. *Journal of Geophysical Research: Oceans*, *121*(7), 4474–4486. https://doi.org/10.1002/2016jc011768
Onorato, M., Residori, S., Bortolozzo, U., Montina, A., & Arecchi, F. T. (2013). Rogue waves and their generating mechanisms in different physical contexts. *Physics Reports*, *528*(2), 47–89. https://doi.org/10.1016/j.physrep.2013.03.001
Onorato, M., Waseda, T., Toffoli, A., Cavaleri, L., Gramstad, O., Janssen, P., et al. (2009). Statistical properties of directional ocean waves: The role of the modulational instability in the formation of extreme events. *Physical Review Letters*, *102*(11), 114502. https://doi.org/10.1103/physrevlett.102.114502
Peregrine, D. H. (1976). Interaction of water waves and currents. *Advances in Applied Mechanics*, *16*, 9–117.
Phillips, W. R. (2002). Langmuir circulations beneath growing or decaying surface waves. *Journal of Fluid Mechanics*, *469*, 317–342. https://doi.org/10.1017/s0022112002001908
Pizzo, N., Lenain, L., Rømcke, O., Ellingsen, S. Å., & Smeltzer, B. K. (2023). The role of Lagrangian drift in the geometry, kinematics and dynamics of surface waves. *Journal of Fluid Mechanics*, *954*, R4. https://doi.org/10.1017/jfm.2022.1036
Pizzo, N., & Melville, W. K. (2016). Wave modulation: The geometry, kinematics, and dynamics of surface-wave packets. *Journal of Fluid Mechanics*, *803*, 292–312. https://doi.org/10.1017/jfm.2016.473
Qiao, F., Yuan, Y., Ezer, T., Xia, C., Yang, Y., Lü, X., & Song, Z. (2010). A three-dimensional surface wave–ocean circulation coupled model and its initial testing. *Ocean Dynamics*, *60*(5), 1339–1355. https://doi.org/10.1007/s10236-010-0326-y
Quinn, B. E., Toledo, Y., & Shrira, V. I. (2017). Explicit wave action conservation for water waves on vertically sheared flows. *Ocean Modelling*, *112*, 33–47. https://doi.org/10.1016/j.ocemod.2017.03.003
Ribal, A., & Young, I. R. (2019). 33 years of globally calibrated wave height and wind speed data based on altimeter observations. *Scientific Data*, *6*(1), 77. https://doi.org/10.1038/s41597-019-0083-9
Romero, L., Lenain, L., & Melville, W. K. (2017). Observations of surface wave–current interaction. *Journal of Physical Oceanography*, *47*(3), 615–632. https://doi.org/10.1175/jpo-d-16-0108.1
Shchepetkin, A. F., & McWilliams, J. C. (2005). The regional oceanic modeling system (ROMS): A split-explicit, free-surface, topography-following-coordinate oceanic model. *Ocean Modell*, *9*(4), 347–404. https://doi.org/10.1016/j.ocemod.2004.08.002
Shrira, V. I. (1993). Surface waves on shear currents: Solution of the boundary-value problem. *Journal of Fluid Mechanics*, *252*, 565–584. https://doi.org/10.1017/s002211209300388x
Smith, J. A. (2006). Observed variability of ocean wave Stokes drift, and the Eulerian response to passing groups. *Journal of Physical Oceanography*, *36*(7), 1381–1402. https://doi.org/10.1175/jpo2910.1
Steer, J. N., Borthwick, A. G. L., Stagonas, D., Buldakov, E., & van den Bremer, T. S. (2020). Experimental study of dispersion and modulational instability of surface gravity waves on constant vorticity currents. *Journal of Fluid Mechanics*, *884*, A40. https://doi.org/10.1017/jfm.2019.951
Stewart, R. H., & Joy, J. W. (1974). HF radio measurements of surface currents. *Deep-Sea Research and Oceanographic Abstracts*, *21*(12), 1039–1049. https://doi.org/10.1016/0011-7471(74)90066-7
Suzuki, N., & Fox-Kemper, B. (2016). Understanding Stokes forces in the wave-averaged equations. *Journal of Geophysical Research: Oceans*, *121*(5), 3579–3596. https://doi.org/10.1002/2015jc011566
Thomas, R., Kharif, C., & Manna, M. (2012). A nonlinear Schrödinger equation for water waves on finite depth with constant vorticity. *Physics of Fluids*, *24*(12). https://doi.org/10.1063/1.4768530
Thorpe, S. (2004). Langmuir circulation. *Annual Review of Fluid Mechanics*, *36*(1), 55–79. https://doi.org/10.1146/annurev.fluid.36.052203.071431
Toffoli, A., & Bitner-Gregersen, E. M. (2017). Types of ocean surface waves, wave classification. *Encyclopedia of Maritime and Offshore Engineering*, *1–8*, 1–8. https://doi.org/10.1002/9781118476406.emoe077
Toffoli, A., Waseda, T., Houtani, H., Cavaleri, L., Greaves, D., & Onorato, M. (2015). Rogue waves in opposing currents: An experimental study on deterministic and stochastic wave trains. *Journal of Fluid Mechanics*, *769*, 277–297. https://doi.org/10.1017/jfm.2015.132
Trulsen, K., Kliakhandler, I., Dysthe, K. B., & Velarde, M. G. (2000). On weakly nonlinear modulation of waves on deep water. *Physics of Fluids*, *12*(10), 2432–2437. https://doi.org/10.1063/1.1287856
Trulsen, K., & Stansberg, C. T. (2001). Spatial evolution of water surface waves: Numerical simulation and experiment of bichromatic waves. In *Isope international ocean and polar engineering conference*. ISOPE–I.
van den Bremer, T., Whittaker, C., Calvert, R., Raby, A., & Taylor, P. (2019). Experimental study of particle trajectories below deep-water surface gravity wave groups. *Journal of Fluid Mechanics*, *879*, 168–186. https://doi.org/10.1017/jfm.2019.584
van den Bremer, T. S., & Breivik, Ø. (2018). Stokes drift. *Philosophical Transactions of the Royal Society A*, *376*(2111), 20170104. https://doi.org/10.1098/rsta.2017.0104

White, B. S., & Fornberg, B. (1998). On the chance of freak waves at sea. *Journal of Fluid Mechanics*, *355*, 113–138. https://doi.org/10.1017/s0022112097007751

Wu, J. (1983). Sea-surface drift currents induced by wind and waves. *Journal of Physical Oceanography*, *13*(8), 1441–1451. https://doi.org/10.1175/1520-0485(1983)013<1441:ssdcib>2.0.co;2

Wu, L., Staneva, J., Breivik, Ø., Rutgersson, A., Nurser, A. G., Clementi, E., & Madec, G. (2019). Wave effects on coastal upwelling and water level. *Ocean Modelling*, *140*, 101405. https://doi.org/10.1016/j.ocemod.2019.101405

Zakharov, V. E. (1968). Stability of periodic waves of finite amplitude on the surface of a deep fluid. *Journal of Applied Mechanics and Technical Physics*, *9*(2), 190–194. https://doi.org/10.1007/bf00913182

Zhang, J., Ma, Y., Tan, T., Dong, G., & Benoit, M. (2023). Enhanced extreme wave statistics of irregular waves due to accelerating following current over a submerged bar. *Journal of Fluid Mechanics*, *954*, A50. https://doi.org/10.1017/jfm.2022.1022

Zheng, Z., Li, Y., & Ellingsen, S. Å. (2023). Statistics of weakly nonlinear waves on currents with strong vertical shear. *Physical Review Fluids*, *8*(1), 014801. https://doi.org/10.1103/physrevfluids.8.014801

Zheng, Z., Li, Y., & Ellingsen, S. Å. (2024). Dispersive wave focusing on a shear current. Part 2: Nonlinear effects. ((submitted to water waves, under review)).

Zippel, S., & Thomson, J. (2017). Surface wave breaking over sheared currents: Observations from the Mouth of the Columbia River. *Journal of Geophysical Research: Oceans*, *122*(4), 3311–3328. https://doi.org/10.1002/2016jc012498

Zippel, S. F., Farrar, J. T., Zappa, C. J., & Plueddemann, A. J. (2022). Parsing the kinetic energy budget of the ocean surface mixed layer. *Geophysical Research Letters*, *49*(2). https://doi.org/10.1029/2021gl095920

References From the Supporting Information

Li, Y., & Chabchoub, A. (2024). How currents trigger extreme sea waves. The roles of Stokes drift, Eulerian return flow, and a background flow in the open ocean. *Geophysical Research Letters*. https://doi.org/10.1029/2023GL107381